УДК 537.525.7

Тепловое состояние неохлаждаемого кварцевого разрядного канала мощного высокочастотного индукционного плазмотрона

А.В. Чаплыгин, С.А. Васильевский, С.С. Галкин, А.Ф. Колесников

*Институт проблем механики им. А.Ю. Ишлинского РАН,
Россия, Москва, 119526, пр-т Вернадского, д. 101, корп. 1*

chaplygin@ipmnet.ru

Аннотация

Исследовано тепловое состояние неохлаждаемого кварцевого разрядного канала ВЧ-плазмотрона ВГУ-4 при мощности ВЧ-генератора по анодному питанию 45 и 70 кВт для трех рабочих газов (воздух, углекислый газ, азот). Проведены эксперименты с целью получения полей температур разрядного канала в зависимости от массового расхода рабочего газа. Максимальная температура стенки разрядного канала наблюдалась в плазме углекислого газа. На основе уравнений Навь–Стокса и упрощенных уравнений Максвелла проведено численное моделирование течения индукционной плазмы для условий экспериментов. Показано, что влияние различных вариантов задания температурных граничных условий для кварцевой стенки на расчетные параметры потока воздушной плазмы у выходного сечения канала незначительно. Результаты расчета температурных полей для плазмы воздуха и азота оказались близкими, что согласуется с экспериментом. Расчетные изолинии функции тока и изотермы соответствуют теоретически предсказанным Ю.П. Райзером.

Ключевые слова: ВЧ-плазмотрон, индукционный разряд, кварцевый разрядный канал
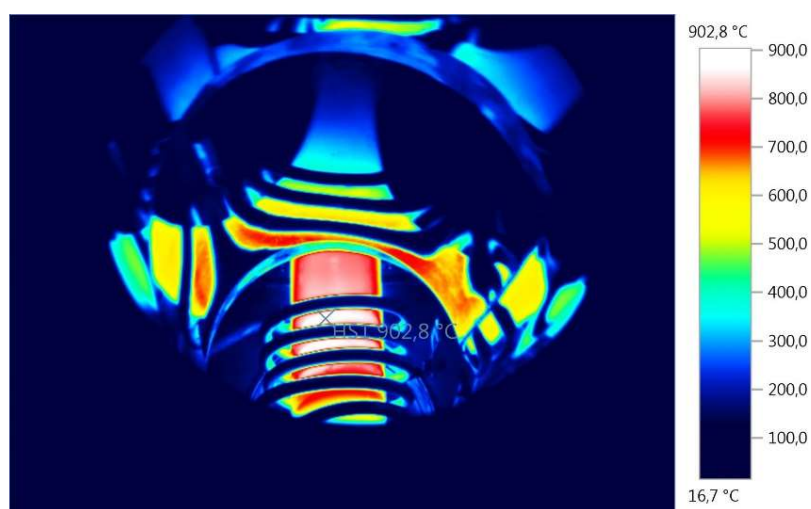
Типичное поле температур кварцевого разрядного канала при постоянном массовом расходе (2.4 г/с) углекислого газа (мощность ВЧ-генератора по анодному питанию $N_{ap} = 70$ кВт)

Thermal state of uncooled quartz discharge channel of powerful high-frequency induction plasmatron

A.V. Chaplygin, S.A. Vasil'evskii, S.S. Galkin, A.F. Kolesnikov

Ishlinsky Institute for Problems in Mechanics RAS,
Moscow, 119526, Russia

chaplygin@ipmnet.ru

Abstract

This paper studies the thermal state of VGU-4 HF-plasmatron uncooled quartz discharge channel at HF-generator anode power values of 45 and 70 kW for three working gases (air, carbon dioxide and pure nitrogen).Experiments were carried out to obtain temperature fields of discharge channel at different working gas mass flow rate. Maximum wall temperatures were observed in carbon dioxide plasma. Inductively coupled plasma flow numerical modeling was made on the basis of Navier − Stokes and simplified Maxwell equations for the experimental conditions. It was shown that the influence of different quartz wall temperature boundary conditions on the calculated air plasma flow parameters at the channel exit section is negligible. The calculation results of temperature fields for nitrogen and air plasma were close, which is in accordance with the experiment. Calculated stream function isolines and isotherms are in accordance with the schematic view proposed by Yu.P. Raizer.

Keywords: HF-plasmatron, induction discharge, quartz discharge channel

1. Introduction

Beginning of extensive applications of electrodeless plasmatrons in technology was initiated by G.I. Babat [1, 2]. In an electrodeless plasma torch, developed by T.B. Reed [3, 4] spinning of the gas flow in tangent direction relate to a discharge tube was used. In this case the main mass of the gas moves along a tube wall and pushes the plasma ball, where temperature reaches 10000 K and above, back from the wall. Such device construction provides capability to work continuously during long time without water-cooling of a discharge tube.

Detailed information about experiments and applications of the low power electrodeless discharge can be found in [5, 6]. Yu.P. Razer mentioned in [5] that in those time technical progress leaved behind understanding physical essence of electrodeless discharge phenomenon and theory.

Applications of HF-plasmatrons for simulation of aerodynamic heating for atmospheric re-entry conditions were initiated by M.I. Yakushin [6, 7] in Institute for Problems in Mechanics of Academy of Sciences USSR. First version of the HF-plasmatron developed by M.I. Yakushin worked at atmospheric pressure using air flow swirling at the entrance of discharge channel and without cooling quartz tube. In eighties technical development of electrodeless plasmatrons have been proceeded in directions of enlargement of discharge channel size and HF-generator power up to 1 MW. Under M.I. Yakushin leadership four HF-plasmatrons of VGU family with cooled-free discharge channels have been constructed at IPM RAS. At the present time in IPM RAS the two HF-plasmatrons VGU-3 and VGU-4 of 1 MW and 100 kW power are in operation [8−10]. These devices are included in composition of Unique Scientific Facility «High-frequency inductive plasmatrons VGU-3 and VGU-4» (https://ckp-rf.ru/usu/441568/).

In 1969 Yu.P. Raizer published basic theory of electrodeless discharge in motionless plasma and stationary HF-discharge in gas flow [5]. Parameters of air and argon plasma flows at atmospheric pressure and HF-generator powers 21.3 and 5.5 kW in Yakushin's plasmatron [6, 7] were

considered by Yu.P. Raizer, when this theory has been built [5]. Quantitative theory was built on the basis of the problem of discharge normal propagation. In the framework of the 1-D theory the question about geometry of discharge in swirling flow of complicated configuration remained to be unsolved. Answers regarding structure of swirling zone in plasma ball have been obtained later as result of CFD modeling inductively coupled plasma flows on basis of Navier − Stokes equations and Maxwell equations.

The VGU-3 plasmatron of 1 MW class is the most powerful facility of the VGU series. It is used for testing of the large-scale samples of thermal protection materials and full-scale elements of thermal protection systems. The VGU-4 facility application is directed to research work in the area of heat exchange between dissociated flows and different materials. The VGU-4 and VGU-3 plasmatrons are described in details in [11]. Their common feature is the use of quartz discharge channels without any forced cooling. Quartz has high thermal resistance. However, operation of powerful plasmatron at low mass flow rate of gas can cause overheating and melting of quartz tube. For this reason, it is important to investigate the temperature fields of the quartz discharge channel at different mass flow rates and gas composition depending on the supplied power. Thermal regimes of the discharge channel wall of the 1 MW VGU-3 plasmatron were shown in [12]. In the present work the thermal state of VGU-4 HF-plasmatron uncooled quartz discharge channel was studied.

2. Experiment

This study was done in subsonic plasma jets of air, nitrogen and carbon dioxide of the VGU-4 HF-plasmatron with vortex gas stabilization and quartz tube as discharge channel. «Testo 890» thermal imager was used for contactless measurements of discharge channel temperature fields. Spectral sensitivity of the thermal imager is $8 \div 14$ µm, it's temperature range is $350 \div 1200$ °C. The preset value of spectral emissivity for quartz «KV» that was used for manufacturing of the discharge channel for the VGU-4 facility was assumed to be 0.94 [13]. The VGU-4 plasmatron has vertical orientation of discharge channel and plasma jet moves vertically upwards. Conceptual sketch of experiment is shown in fig. 1.
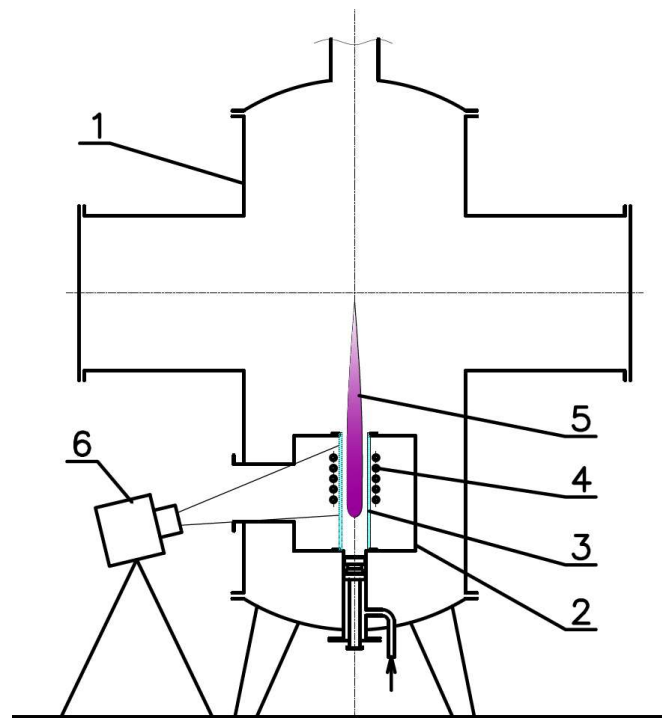
Fig. 1. Conceptual sketch of experiment. 1 − test chamber, 2 – induction chamber, 3 – discharge channel, 4 – inductor, 5 – plasma jet

Quartz discharge channel (3) is placed in the induction chamber (2) and has outer diameter 80 mm and thickness of wall $4 \div 5$ mm. Free subsonic plasma jet (5) is injected into test chamber (1) from exit section of discharge channel. 5-turns water-cooled inductor (4) is 120 mm of length and 120 mm outer diameter. Distance from exit section of discharge channel to upper turn of inductor is 130 mm. Thermal imager (6) is arranged near test chamber and measurements were made through cylindrical tube connected straight to the induction chamber.

Experiments were carried out at pressure in test chamber 50 hPa. Mass flow rate of plasma forming gas through discharge channel was $G = 1.8 \div 3.6$ g/s and was controlled by a «Bronkhorst MV-306» flow meter. Measurements were done at HF-generator anode power (Nap) values of 45 and 70 kW. Dependency of maximum temperature over outer surface of discharge channel versus mass flow rate of gas (air, nitrogen or carbon dioxide) is presented in fig. 2. Maximum temperature over quartz tube determines heat resistance of discharge channel. Choosing a low mass flow rate of gas allows to improve the quality of the jet, but it can lead to heating of the quartz wall to an unacceptably high temperature. A lower mass flow rate leads to a rapid increase in the surface temperature of the discharge channel for air and nitrogen plasma at constant anode power. Despite the lower efficiency of the VGU-4 plasmatron [14], the use of carbon dioxide leads to high temperatures of the discharge channel due to intense radiation [15]. The effect can be reduced by switching to a higher mass flow rate. But the dependence of the quartz tube maximum temperature versus mass flow rate of carbon dioxide is not so strong as for air or nitrogen plasma.
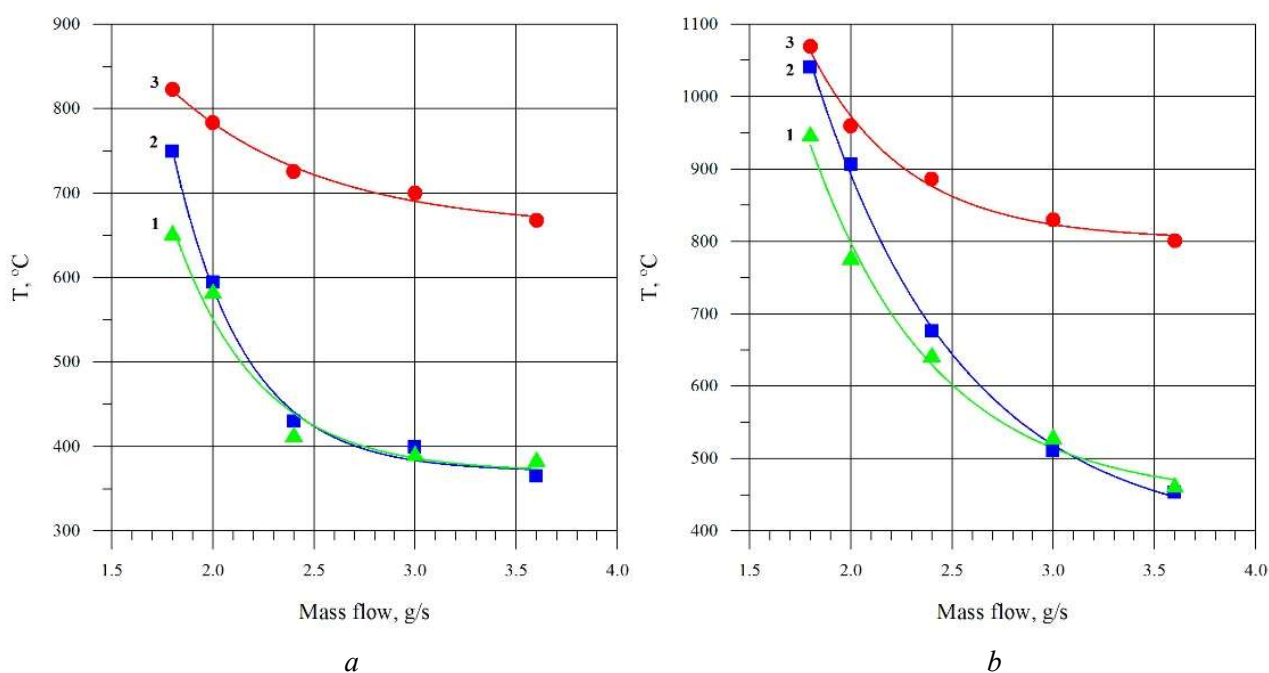
Fig. 2. Maximum temperature over outer surface of quartz discharge channel against mass flow rate of nitrogen (1), air (2) or carbon dioxide (3) through discharge channel at HF-generator anode power (N_{ap}) values of 45 kW (a) and 70 kW (b)

Typical temperature fields of discharge channel for two different gases (air and carbon dioxide) are shown in fig. 3. The temperature fields in the nitrogen plasma were very close to those obtained in the air plasma for the same regime. Temperature fields in nitrogen and air plasma were significantly non-uniform, maximum temperatures took place near exit section of discharge channel. The effect of the gas swirling on the shape of temperature fields was clearly visible. Figure 3b shows that temperature distribution in carbon dioxide plasma is much more uniform, and maximum temperature was observed between 4th and 5th turns of the inductor. This is due to the large contribution of radiation in the heat exchange between the carbon dioxide plasma and the wall of the discharge channel.
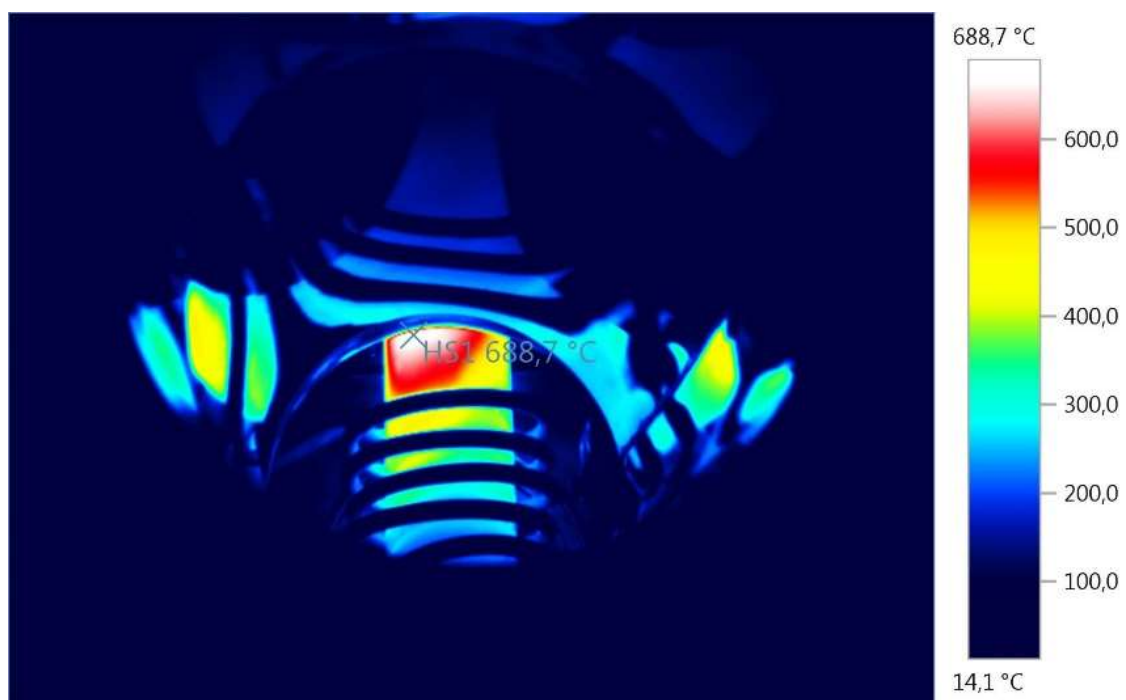
a
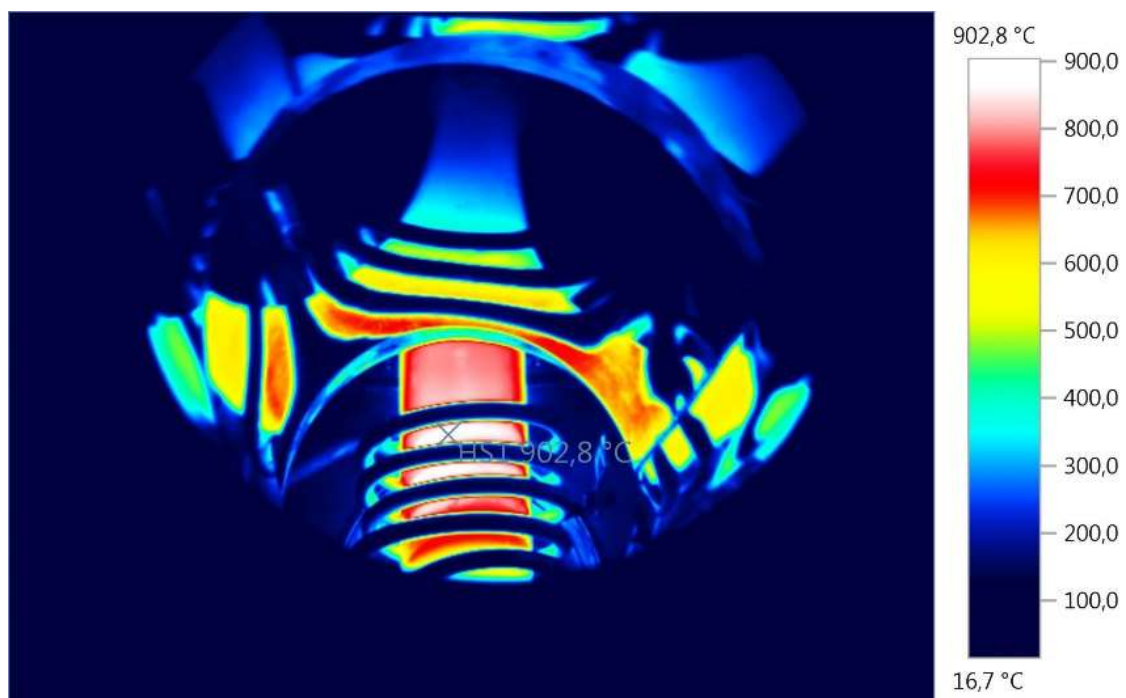
b

Fig. 3. Typical temperature fields of quartz discharge channel at constant mass flow rate (2.4 g/s) of air (*a*) and carbon dioxide (*b*) (HF-generator anode power $N_{ap} = 70$ kW)

3. Numerical modeling

Laboratory of Interaction of Plasma and Radiation with Materials of IPMech RAS developed the program package for complete numerical simulation of subsonic plasma flow (air, nitrogen, oxygen, carbon dioxide, argon) in the induction plasmatron and determination of surface catalycity of testing materials. This integral program package includes the codes Alpha, Beta and Gamma. IPMech approach is based on the fact that the whole flow in the induction plasmatron can be subdivided into three regions: 1) plasma flow within the discharge channel; 2) exhaust jet flow over testing model in test chamber; 3) boundary layer in front of the model stagnation point.

This work is restricted by only the first region (Alpha code). The inductively coupled subsonic laminar plasma flow in the discharge channel is assumed to be under LTE conditions; axial symmetry is assumed also. Cylindrical coordinate system is used to write the governing equations. Alpha is based on numerical solution of Navier−Stokes equations coupled with simplified Maxwell equations for HF electromagnetic field. This simplified model for the electromagnetic field was developed for geometry and experimental conditions of VGU-4 plasmatron.

In the past years the code-to-code validations were made between Alpha code and CFD codes developed in the von Karman Institute for Fluid Dynamics (VKI) in Belgium [16, 17], and in the Moscow Institute for Physics and Technology MIPT [18]. Comparison of Alpha code calculations with CFD code developed in the Institute of Mechanics of the Lomonosov Moscow State University (IM MSU) was made also [19]. Note that IM MSU code was developed for both thermal and chemical nonequilibrium flow. The mentioned code-to-code comparisons were made for the cases of pure argon, air and CO_2 plasma flows in VGU-4 plasmatron, with use of simple geometry of discharge channel – cylindrical quartz tube without conic nozzle. The comparison of our calculation results obtained by Alpha code with IPM experimental data for flow temperature for air and CO_2 working gases was made [20]. In total, the comparisons showed the good accuracy of Alpha code in the range of pressure above 50 hPa and for plasmatron power not very high to avoid the account for plasma radiation.

3.1. Governing equations

3.1.1. Gasdynamics

Alpha code was developed to calculate inductively coupled plasma (ICP) flow within the VGU-4 plasmatron discharge channel - the 80-mm diameter quartz tube with inductor coil over it. Working gas is injected into the channel through the annular inlet slot adjacent to the wall; thickness of the slot is 2 mm. To provide the axial symmetry of the problem, the inductor coil is treated as five separate turns with the same current in each of them. Inductor turns are represented as thin equidistant rings perpendicular to the symmetry axis. Subsonic plasma flow in the discharge channel is assumed to be stationary, laminar and axisymmetric one with swirling in azimuthal direction. The flow is assumed to be under equilibrium conditions (both local thermal and chemical equilibrium is assumed); radiative processes are supposed to be negligible.

The full Navier−Stokes equations written in cylindrical coordinate system are used to simulate ICP flow in the discharge channel. We assume that Navier−Stokes equations are time-averaged with respect to HF oscillations of the inductor current. The resulting governing equations are the two-dimensional equations with account for three velocity components − axial u, radial v, and tangential component w due to the flow spinning, together with energy equation written for the total gas enthalpy h

$$\frac{\partial}{\partial z}(\rho u) + \frac{1}{r}\frac{\partial}{\partial r}(r\rho v) = 0, \qquad (1)$$

$$\frac{\partial}{\partial z}(\rho uu) + \frac{1}{r}\frac{\partial}{\partial r}(r\rho uv) = -\frac{\partial}{\partial z}\left(P + \frac{2}{3}\mu\left[\frac{\partial u}{\partial z} + \frac{1}{r}\frac{\partial rv}{\partial r}\right]\right) +$$
$$+ 2\frac{\partial}{\partial z}\left(\mu\frac{\partial u}{\partial z}\right) + \frac{1}{r}\frac{\partial}{\partial r}\left(r\mu\left(\frac{\partial u}{\partial r} + \frac{\partial v}{\partial z}\right)\right) + F_z \tag{2}$$

$$\frac{\partial}{\partial z}(\rho uv) + \frac{1}{r}\frac{\partial}{\partial r}(r\rho vv) = -\frac{\partial}{\partial r}\left(P + \frac{2}{3}\mu\left[\frac{\partial u}{\partial z} + \frac{1}{r}\frac{\partial rv}{\partial r}\right]\right) +$$
$$+ \frac{\partial}{\partial z}\left(\mu\left(\frac{\partial v}{\partial z} + \frac{\partial u}{\partial r}\right)\right) + \frac{2}{r}\frac{\partial}{\partial r}\left(r\mu\frac{\partial v}{\partial r}\right) - \frac{2\mu v}{r^2} + \frac{\rho w^2}{r} + F_r \tag{3}$$

$$\frac{\partial}{\partial z}(\rho uw) + \frac{1}{r}\frac{\partial}{\partial r}(r\rho vw) = \frac{\partial}{\partial z}\left(\mu\frac{\partial w}{\partial z}\right) + \frac{1}{r}\frac{\partial}{\partial r}\left(r\mu\frac{\partial w}{\partial r}\right) - \frac{\rho vw}{r} - \frac{w}{r^2}\frac{\partial}{\partial r}(r\mu) \tag{4}$$

$$\frac{\partial}{\partial z}(\rho uh) + \frac{1}{r}\frac{\partial}{\partial r}(r\rho vh) = \frac{\partial}{\partial z}\left(\frac{\mu}{\mathrm{Pr}_{eff}}\frac{\partial h}{\partial z}\right) + \frac{1}{r}\frac{\partial}{\partial r}\left(\frac{r\mu}{\mathrm{Pr}_{eff}}\frac{\partial h}{\partial r}\right) + Q_J \tag{5}$$

Here z and r are the axial and radial coordinates; P, ρ, h, μ are the pressure, density, enthalpy and viscosity of equilibrium gas mixture, Pr_{eff} is the effective Prandtl number.

These equations include time-averaged source terms corresponding to HF electromagnetic field influence: F_z, F_r are axial and radial components of the Lorentz force; Q_J is Joule heat production. These source terms are expressed via E_θ − tangential component of the complex amplitude of vortical electric field:

$$F_z = -\frac{\sigma}{2\omega}Re\left\{E_\theta\left(i\frac{\partial E_\theta}{\partial z}\right)^*\right\}, \quad F_r = -\frac{\sigma}{2\omega}\frac{1}{r}Re\left\{E_\theta\left(i\frac{\partial rE_\theta}{\partial r}\right)^*\right\}, \quad Q_J = \frac{\sigma}{2}E_\theta E_\theta^* \tag{6}$$

Here Re means the real part of a complex value, asterisk is the conjugation sign for a complex value; ω is circular frequency of monochromatic electric field; σ is plasma electrical conductivity.

Boundary conditions for gasdynamic equations

All the necessary flow parameters are specified at the discharge channel inlet section. These specified parameters are the following (subscript «0» here refers to parameters of the gas injected into the channel at the channel inlet section):

$\rho_0 u_0(r) = G/A_{SL}$, here G is specified mass flow rate; A_{SL} is area of the annular inlet slot;

$v_0(r) = 0$;

$T_0(r) = 300$ K is the temperature of the injecting gas;

P_0 is the static pressure specified at inlet section at the symmetry axis;

$\theta_0 = 45°$ is the swirl angle of the injecting gas, $w_0/u_0 = tg(\theta_0)$.

Zero values for the velocity components are specified at all rigid surfaces − quartz tube wall, face of the gas injector interface at the channel inlet section; definite values of temperature are specified at all rigid surfaces; in particular, the wall temperature of the quartz tube in general is a function of z: $T_w = T_w(z)$.

Symmetry conditions are applied at the channel axis.

«Soft conditions» are applied at the channel exit section (outlet) $z = Z_c$, i.e. the unknown functions are extrapolating outside the calculation region

$$\frac{\partial u}{\partial z}(Z_c, r) = \frac{\partial v}{\partial z}(Z_c, r) = \frac{\partial w}{\partial z}(Z_c, r) = \frac{\partial h}{\partial z}(Z_c, r) = 0 \tag{7}$$

3.1.2. Electrodynamics

Suppose that HF oscillating inductor current is composed of a single Fourier mode and it produces a monochromatic electric field with complex amplitude

$$\vec{E}(t, z, r) = \vec{E}(z, r) \cdot \exp(-i\omega t), \quad \vec{H}(t, z, r) = \vec{H}(z, r) \cdot \exp(-i\omega t)$$

Here $\omega = 2\pi f$ is the circular frequency; f is the frequency of inductor current; t is the time. Here we use complex values of E and H amplitudes.

The following common assumptions are used: plasma is quasi-neutral; plasma magnetic permeability $\mu = 1$; plasma dielectric constant does not depend on the electromagnetic field and so does not depend on z and r; the displacement current is negligible; inductor coil is represented by a series of parallel current-carrying rings to provide the axial symmetry for the problem; the rings are assumed to be infinitely thin; a single coil current with the same amplitude and phase angle is assumed to oscillate through each of coil rings.

Following [21], we use also the assumption $\partial E_\theta / \partial z \ll \partial E_\theta / \partial r$, that leads (with account for symmetry conditions) to quasi-one-dimensional approximation of Maxwell equations [22−24]:

$$\frac{\mathrm{d}}{\mathrm{d}r}\left(\frac{1}{r}\frac{\mathrm{d}}{\mathrm{d}r}(rE_\theta)\right) = -i\omega\mu_0\sigma E_\theta$$

$$E_z = 0, \quad E_r = 0, \quad i\omega\mu_0 H_z = \frac{1}{r}\frac{\mathrm{d}}{\mathrm{d}r}(rE_\theta) \tag{8}$$

Here E_z, E_r, E_θ are axial, radial and tangential components of the electric field amplitude; H_z is axial component of the magnetic field amplitude; μ_0 is the magnetic constant (vacuum permeability). Equation (8) together with appropriate boundary conditions (9−10) (see below) is used in our method to determine electromagnetic field amplitudes E_θ and H_z.

The quasi-1D approximation is essential simplification for the problem, it leads to boundary value problem for the ordinary differential equation (8) to determine complex amplitude of the electric field $E_\theta(z, r)$; z coordinate is only a parameter in this equation; E_θ depends on z owing to the boundary conditions. In this approximation the axial component of the Lorentz force F_z equals to zero. Note that for the equilibrium plasma it's electric conductivity $\sigma = \sigma(P, T)$, so σ serves here as interface between the gasdynamic and electrodynamic subsystems of the governing equations.

Boundary conditions for the equation (8) are the symmetry condition at the axis

$$E_\theta(z, 0) = 0, \tag{9}$$

and the following condition at the discharge channel wall:

$$r = R_c: \quad \frac{1}{r}\frac{\mathrm{d}}{\mathrm{d}r}(rE_\theta) = i\omega\mu_0 H_{zw0}(z) \tag{10}$$

Here R_c is the channel radius; H_{zw0} is the amplitude of the magnetic field axial component at the channel wall produced only by the inductor current outside the plasma flow.

It is important to note that the comparison of accurate electrodynamic model results [24, 25] (the full two-dimensional Maxwell equations were solved on a far field domain) with our results obtained with use of the quasi-1D model (8−10) demonstrated a good accuracy of this simplified model for VGU-4 plasmatron with relatively thin channel in wide range of operating frequency and pressure. Differences of a few percent between the results were observed in the inlet region and at the mid-coil position; practically no differences were observed at the channel outlet. The comparison made for the VGU-4 discharge channel geometry is reported in details in [16, 26].

3.2. Calculation of thermodynamic and transport properties of equilibrium plasmas

To calculate Navier−Stokes and Maxwell equations, a set of thermodynamic and transport properties is necessary. These properties, including viscosity, thermal conductivity, electrical conductivity, can be calculated in advance for the case of chemical equilibrium mixture as functions of pressure and temperature. We use here the standard assumptions:

− elementary composition of equilibrium mixture is constant (concentrations of chemical elements C_j^* do not vary in a flow); plasma is quasi neutral, $C_E^* = 0$;

− effects of non-ideal gas and plasma are not accounted;

− high frequency electromagnetic field does not influence the transport properties.

SoVA code [27] was developed to calculate chemical composition and transport properties of equilibrium multicomponent mixture; in general, the mixture consists of CO_2 and air with $N = 22$ components produced by $L = 5$ chemical elements (including the electron "e"):

O, N, C, Ar, e, O_2, N_2, CO_2, NO, CO,
O^+, N^+, C^+, Ar^+, O_2^+, N_2^+, CO_2^+, NO^+, CO^+, O^{++}, N^{++}, C^{++}.
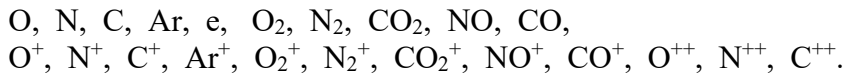
Calculations can be made in the range of pressure and temperature: $0.001 \leq P \leq 10$ atm; $300 \leq T \leq 20000$ K. The calculated output thermodynamic properties are: equilibrium mole fractions x_i; heat capacities under constant pressure C_{pi} ($i = 1,...N$); mixture molecular weight m, density ρ, specific enthalpy h, specific heat capacity under constant pressure C_p; reaction heat capacity C_{pr}; effective (or total) heat capacity under constant pressure $C_{p\,\text{eff}} = C_p + C_{pr}$ for equilibrium gas mixture. To calculate equilibrium reaction rate constants K_{pr} and heat production Q_r, enthalpies h_i and heat capacities C_{pi} of species ($i = 1, ..., N$), we use the approximations for the reduced Gibbs energy $\Phi_i(T)$ [28]. Here «r» is a reaction index, $r = 1,...,R$, $R = N - L$ is the number of independent reactions in the mixture. Additional approximations for O_2, N_2, CO_2 were developed for the low temperatures $T < 1000$ K to calculate species heat capacities and enthalpies with higher accuracy. Additional approximations were developed also for the second ions.

The calculated output transport properties are: viscosity $\mu(\xi)$; translational thermal conductivity $\lambda_{\text{tr}}(\xi)$; thermal conductivity due to molecules internal energy transfer λ_{int}; electrical conductivity $\sigma(\xi)$; thermal conductivity due to equilibrium chemical reactions $\lambda_{\text{R}}(\xi)$; effective thermal conductivity $\lambda_{\text{eff}}(\xi) = \lambda_{\text{tr}}(\xi) + \lambda_{\text{int}} + \lambda_{\text{R}}(\xi)$; effective Prandtl number $\text{Pr}_{\text{eff}} = C_{p\text{eff}}\mu/\lambda_{\text{eff}}$. Thermodiffusion and multicomponent diffusion properties are calculated also. Here ξ is the order of approximation by Sonine polynomials, i.e. the number of terms in Sonine polynomial expansions of Boltzmann equation solution that provide convergence in Chapman−Enskog method, λ_{tr} is the "true" thermal conductivity corresponding to the formula for the full heat flux [29]. Calculations of transport properties are made by the precise formulas of Chapman−Enskog method [29, 30]. The term λ_{int} is calculated with use of Eucken formula. To calculate transport coefficients for neutral gases, the first non-zero approximation ($\xi = 1$ for viscosity, $\xi = 2$ for thermal conductivity) is rather accurate, but for ionized gas mixture this approximation can lead to error, up to $\sim 50\,\%$ error for air when degree of ionization is high [31]. Therefore, our calculations have been made with $\xi = 2$ for viscosity, $\xi = 4$ for other transport coefficients to provide high accuracy. The formula from [29] used to calculate $\lambda_{\text{tr}}(\xi), \xi = 4$, is presented below as an example

$$\lambda_{tr}(4) = -\frac{75}{8}\frac{k\,n}{\det\|q\|} \times \begin{vmatrix} 0 & x_s & 0 & 0 \\ x_r & q_{rs}^{11} & q_{rs}^{12} & q_{rs}^{13} \\ 0 & q_{rs}^{21} & q_{rs}^{22} & q_{rs}^{23} \\ 0 & q_{rs}^{31} & q_{rs}^{32} & q_{rs}^{33} \end{vmatrix}, \quad \det\|q\| = \begin{vmatrix} q_{rs}^{11} & q_{rs}^{12} & q_{rs}^{13} \\ q_{rs}^{21} & q_{rs}^{22} & q_{rs}^{23} \\ q_{rs}^{31} & q_{rs}^{32} & q_{rs}^{33} \end{vmatrix}$$

Here q_{rs}^{mp} is square matrixes of $N \times N$ order, their elements are expressed by the linear combinations of the collision integrals $\Omega_{ij}^{(l,s)}$ [32]; $\det\|q\|$ is determinant of the order of $3N \times 3N$. Details of calculation technique and results obtained for air plasma have been presented in [31]. Note that the

exploited formulas [29] for transport properties are essentially more convenient for calculations than the classic formulas [32] of Chapman−Enskog method, because the formulas from [32] are more complicated and they use the higher order determinants: $N\xi \times N\xi$ instead of $N(\xi-1) \times N(\xi-1)$.

To calculate transport coefficients, the collision integrals $\Omega_{ij}^{(l,s)}(T)$ are necessary. They are determined on the basis of the best available data for various pairs of particles according to the recommendations [33, 34].

As an example, fig. 4 shows the calculated effective Prandtl number $\mathrm{Pr}_{\mathrm{eff}}$ (a) and electrical conductivity σ (b) for $P = 0.1$ atm for the three mixtures: air, CO_2, and pure nitrogen.

Tables of the necessary thermodynamic and transport properties for chemically equilibrium mixtures (air, CO_2, and pure nitrogen) have been calculated with use of SoVA code to apply in Alpha code.
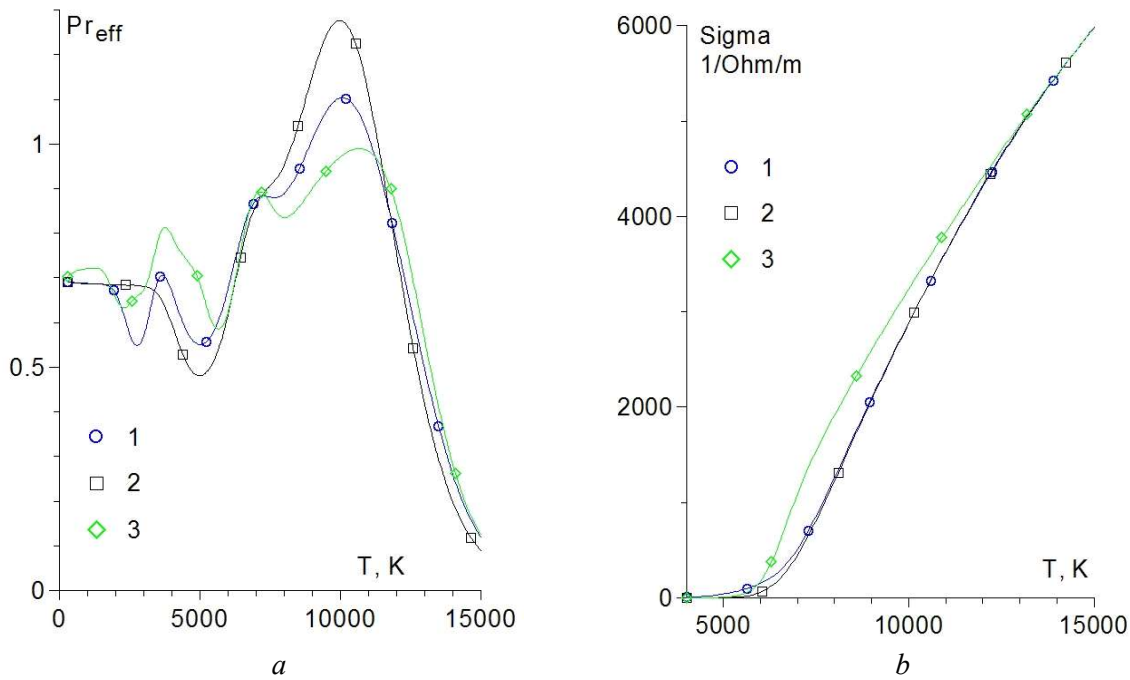
Fig. 4. Effective Prandtl number (a) and electrical conductivity (b) calculated for three gas mixtures: air (1), nitrogen (2), CO_2 (3)

3.3.   Numerical solution technique

Alpha solves finite-difference approximations to the governing equations with use of the control volumes method and SIMPLE algorithm of Patankar and Spalding [35, 36]. Convective terms are approximated by the finite differences with the first order accuracy. Some necessary modifications of the Patankar & Spalding method were made to provide the convergence of iterations for complicated ICP flow with large vortices [37]. In particular, the unknown functions are determined with use of additional under-relaxation procedure to increase stability of the solution technique.

Non-uniform rectangular finite-difference grid is used both in axial and radial directions. The grid is condensed in radial direction near the torch wall; the grid is condensed in axial direction near the torch inlet section and within the inductor region. Thomas algorithm («sweep» algorithm) for 3-diagonal matrix equations with use of complex variables is applied to solve the boundary value problem for the simplified Maxwell equations (8)−(10) to obtain the complex value of the electric field amplitude E_θ. Value of the inductor current is determined in process of iterations by the prescribed value of power input in plasma N_{pl}. As to a value of N_{pl} itself, it should be specified by both the measured value of anode power N_{ap} and the plasmatron efficiency η_{eff} obtained from special experimental measurements: $N_{\mathrm{pl}} = \eta_{\mathrm{eff}*} N_{\mathrm{ap}}$.

The necessary thermodynamic and transport properties are determined simultaneously in the process of numerical solution for each grid point by the interpolation procedure across the previously calculated tables.

3.4. Computation results for the test regimes

The two numerical investigations are presented below for the flow and electromagnetic field within the discharge channel of VGU-4 induction plasmatron. The first is the investigation of the influence of discharge channel wall temperature T_w on plasma parameters and electromagnetic field; the second is the investigation of the influence of working gas − air, CO_2, and pure nitrogen − on plasma parameters.

The geometry of VGU-4 discharge channel is presented above. The inductor current frequency is 1.76 MHz. All computations are made for the experimental conditions, at a constant working gas mass flow rate $G = 2.4$ g/s and pressure in the pressure chamber of 50 hPa.

3.5. Influence of the discharge channel wall temperature on plasma parameters

Here the computations are made for air working gas for the power $N_{ap} = 70$ kW, for the three variants of boundary conditions for the wall temperature T_w :

1) $T_{wentry} = T_{wq1} = T_{wq2} = 300$ K (standard);

2) $T_{wentry} = T_{wq1} = T_{wq2} = 747$ K (constant temperature obtained from averaged value of temperature measurements for the corresponding experimental regime);

3) $T_{wentry} = T_{wq1} = 333$ K, $T_{wq2} = 962$ K (linear distribution of temperature along the quartz tube obtained from the approximation of the experimental measurements).

Here T_{wentry} is the temperature of the low interface at the channel inlet section; T_{wq1} and T_{wq2} is the temperature at the beginning (inlet section) and at the end of the quartz tube (exit section).

Some results of the comparison of computation results for the three cases of T_w boundary conditions are shown in the figures 5−6.
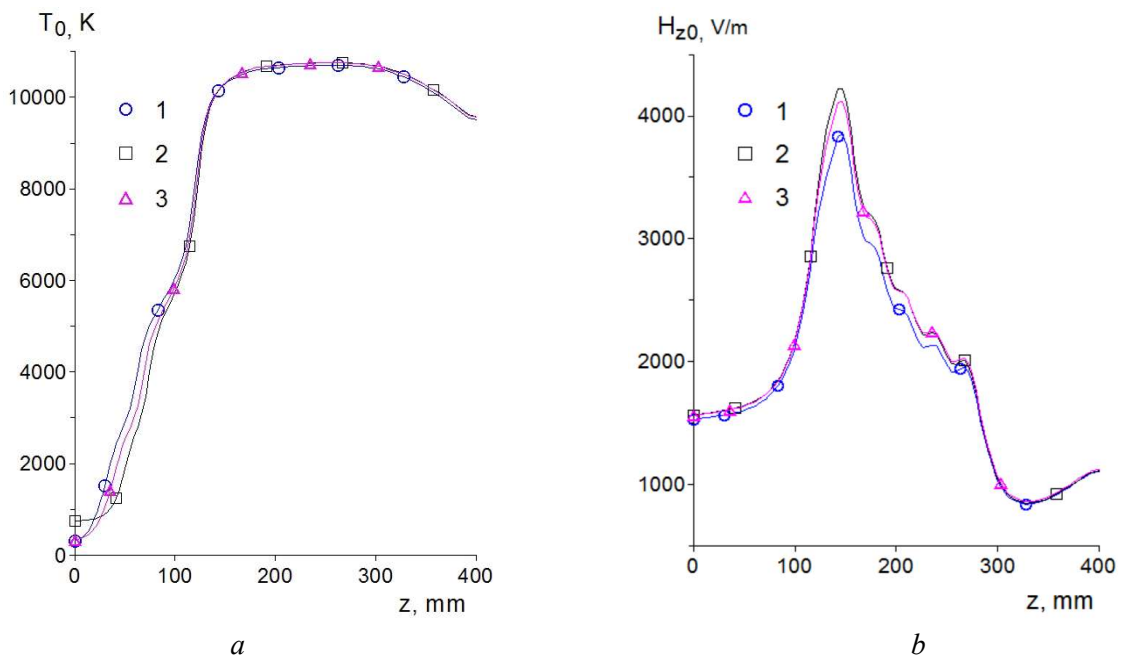
Fig. 5. Distribution of gas temperature T_0 (*a*) and axial component of the magnetic field amplitude H_{z0} (*b*) along the channel axis for the three cases of T_w boundary conditions: standard $T_w = 300$ K (1), constant $T_w = 747$ K (2), linear distribution $T_w(z)$ (3)
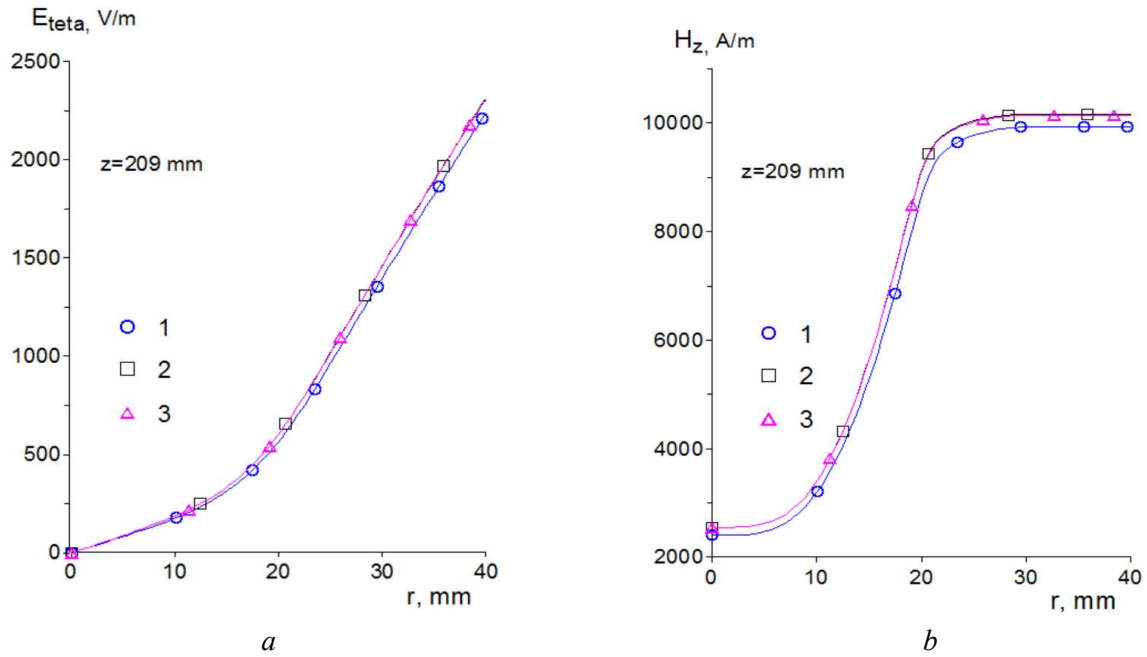
Fig. 6. Radial profiles of tangential component of electric field amplitude E_θ (*a*) and axial component of magnetic field amplitude H_z (*b*) in the section $z = 209$ mm inside the inductor region for the three cases of T_w boundary conditions: standard $T_w = 300$ K (1), constant $T_w = 747$ K (2), linear distribution $T_w(z)$ (3)

From the comparison of computation results for the three cases of T_w boundary conditions the following conclusions can be made.

The influence of T_w on gas parameters at the channel exit section is small, about 1 % for gas temperature and enthalpy and 3 % for flow velocity.

The influence of T_w on flow field (stream lines, isotherms) is small in the region from the inductor to the channel exit. The influence of T_w on flow field in the region from the channel inlet section to the inductor is appreciable but not large.

The influence of T_w on the velocity distribution $u_0(z)$ along the flow axis is negligible; the influence of T_w on the temperature distribution $T_0(z)$ is appreciable in the beginning of the channel near the inlet section and is small in the inductor region and at the exit section, see fig. 5, *a*. The influence of T_w on the magnetic field amplitude $H_{z0}(z)$ at the flow axis is appreciable (up to 9 %) in the inductor region and is small at the end of the channel, see fig. 5, *b*.

The influence of T_w on the magnetic field amplitude $H_z(r)$ at the section $z = 209$ mm inside the inductor region is $2 \div 6$ %. The influence of T_w on the electric field amplitude $E_\theta(r)$ at the section $z = 209$ mm is small, up to 3 % at the wall. Note that $H_z(r)$ and $E_\theta(r)$ for the cases 2 ($T_w = 747$ K) and 3 (linear distribution of $T_w(z)$) are nearly the same, see fig. 6.

3.6. Influence of working gas - air, CO₂, and pure nitrogen - on plasma parameters

Isolines of the dimensionless stream function and isotherms in VGU-4 discharge channel for the test regimes with the three working gases are shown in figures 7−12. The tests and calculations were made for the power values of 45 and 70 kW for each working gas at a constant mass flow rate of 2.4 g/s and pressure in the pressure chamber of 50 hPa. Isolines of the dimensionless stream function f are shown in top parts of the figures (*a*) to visualize the complicated structure of ICP vortical flow: secondary vortex is formed near the inlet section, and large primary vortex with negative values of stream function f is formed between the secondary vortex and the inductor region. Note that dimensionless stream function $f(z,r)$ reaches its maximum value $f = 1$ at the torch wall.

The isotherms are shown in the bottom parts of the figures (*b*), temperature values are given in K. The maximum of temperature is located within the inductor region close to the symmetry axis. From the comparison of isotherms for different gases it is clear that the temperatures in carbon

dioxide plasma are lower at the same power both in the discharge region and at the exit section of the discharge channel. The computation results for nitrogen and air plasmas are close, and it is in accordance with the experiment, where similar temperature fields were obtained.

Variation of pressure within the discharge channel is relatively small for all cases. For example, $\Delta P = P(z,r) - P_0$ changes from -93 Pa at the symmetry axis at the channel exit section to $+47$ Pa near the wall before the inductor region for the air plasma case, $N_{ap} = 70$ kW, $P_0 = 5000$ Pa. Isolines of pressure variation $\Delta P = P(z,r) - P_0$ in IPG-4 discharge channel for air plasma are shown in fig. 13.

Radial profiles of calculated plasma parameters in the discharge channel exit section for VGU-4 regime $N_{ap} = 70$ kW are shown in fig. 14: axial velocity $u_c(r) = u(Z_C, r)$ (a); enthalpy $h_c(r) = h(Z_C, r)$ (b).
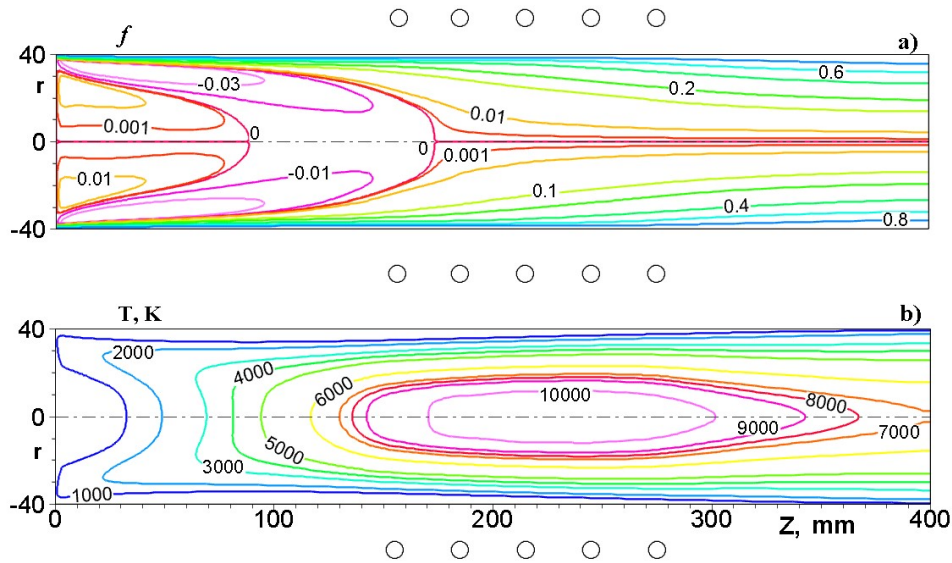
Fig. 7. Isolines of stream function f (a) and isotherms T, K (b) in VGU-4 discharge channel for $N_{ap} = 45$ kW, air
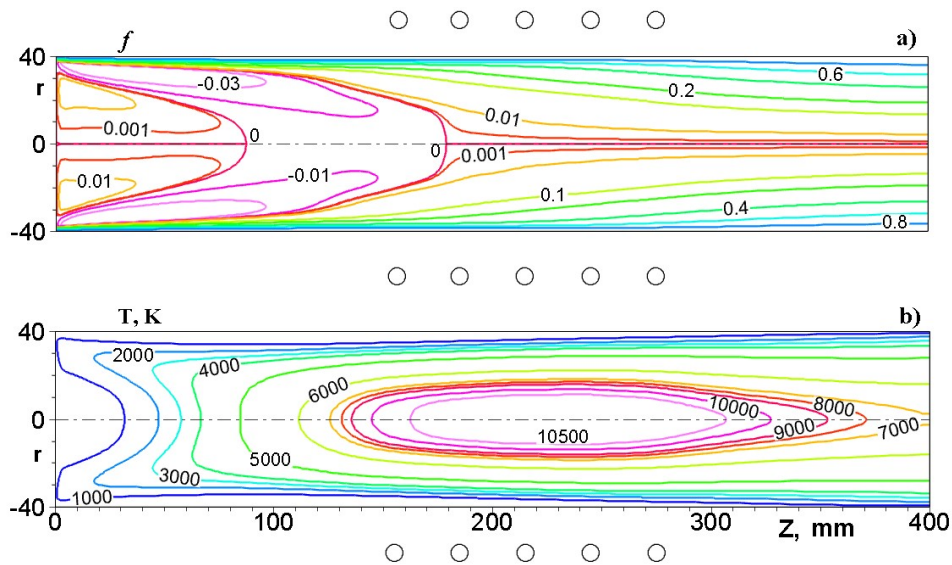
Fig. 8. Isolines of stream function f (a) and isotherms T, K (b) in VGU-4 discharge channel for $N_{ap} = 45$ kW, pure nitrogen

13
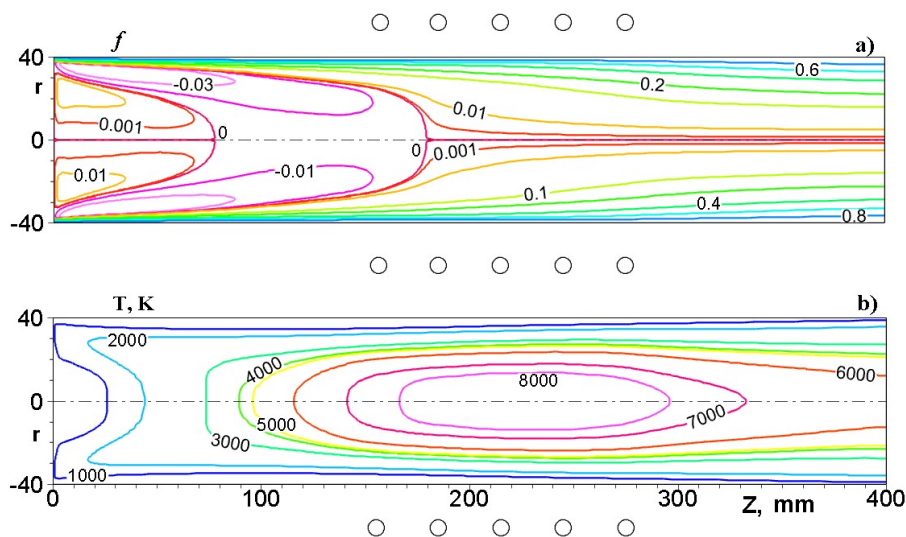
Fig. 9. Isolines of stream function f (a) and isotherms T, K (b) in VGU-4 discharge channel for $N_{ap} = 45$ kW, CO_2
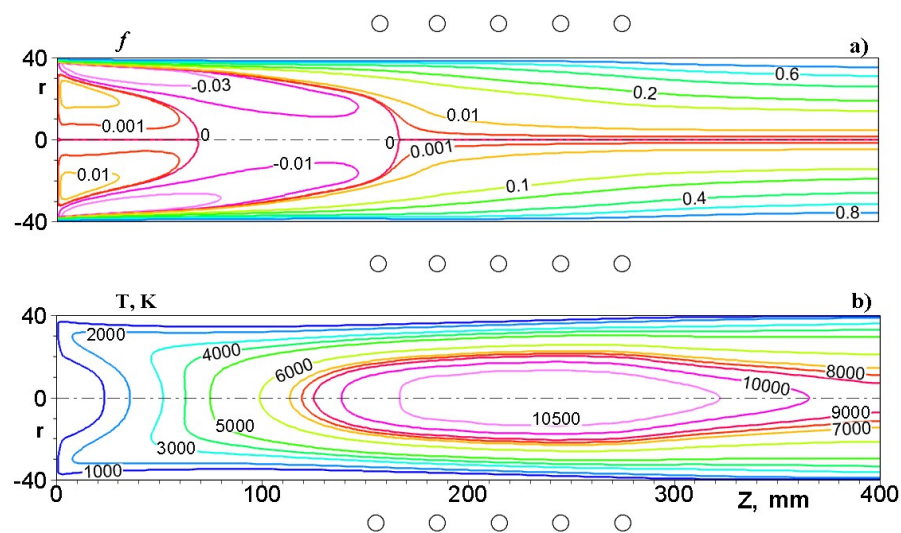
Fig. 10. Isolines of stream function f (a) and isotherms T, K (b) in VGU-4 discharge channel for $N_{ap} = 70$ kW, air
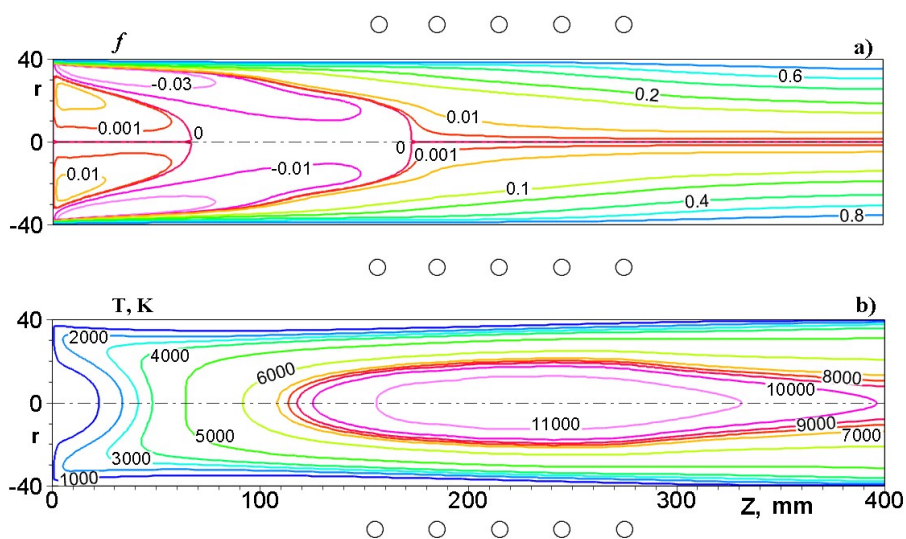
Fig. 11. Isolines of stream function f (a) and isotherms T, K (b) in VGU-4 discharge channel for $N_{ap} = 70$ kW, pure nitrogen

14
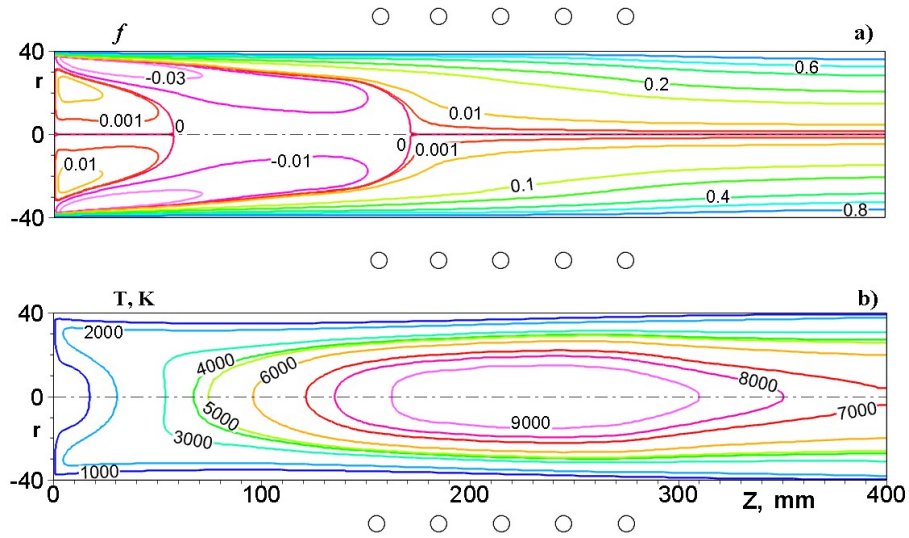
Fig. 12. Isolines of stream function f (*a*) and isotherms T, K (*b*) in VGU-4 discharge channel for $N_{ap} = 70$ kW, CO_2
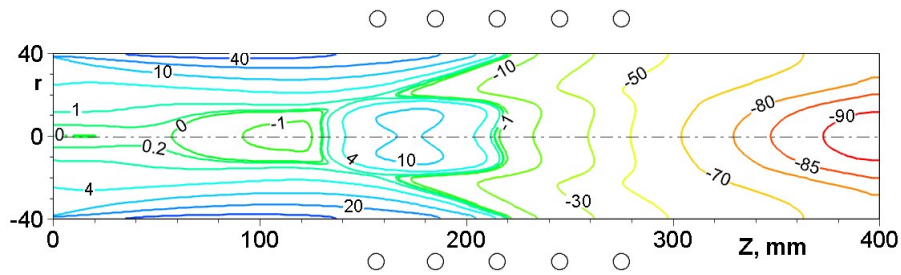
Fig. 13. Isolines of pressure variation $\Delta P = P(z, r) - P_0$ in IPG-4 discharge channel for $N_{ap} = 70$ kW, air, $P_0 = 5000$ Pa.
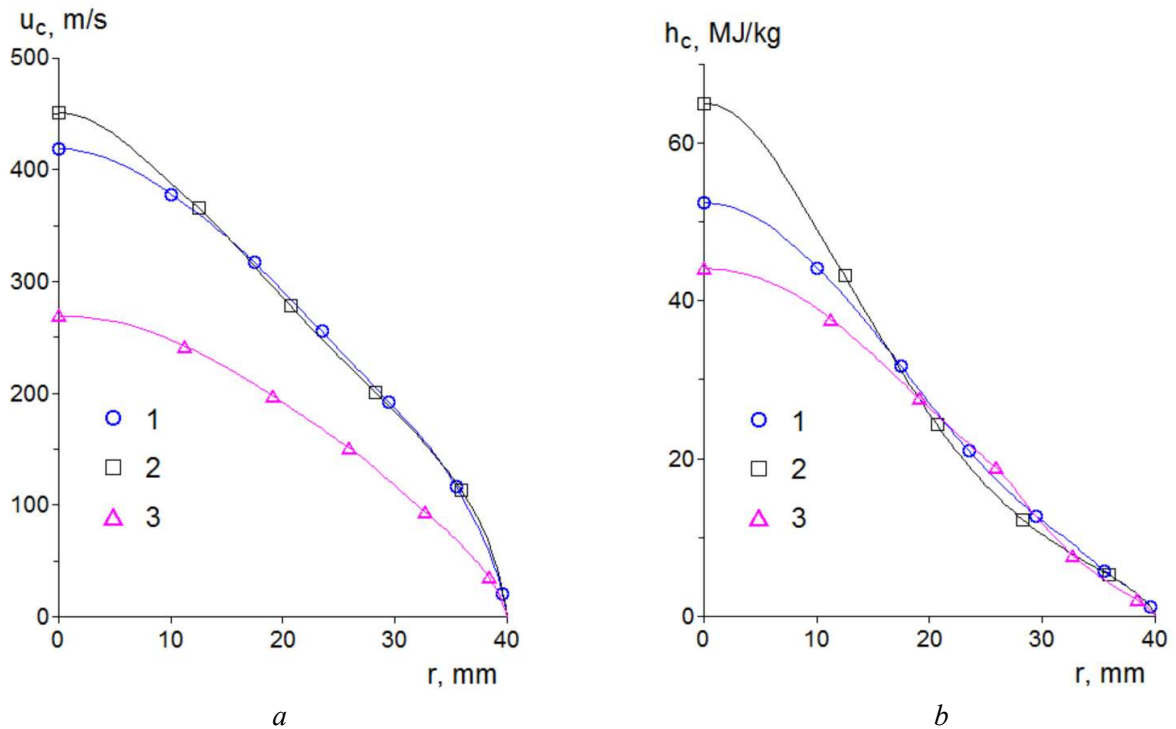
Fig. 14. Radial profiles of axial velocity (*a*) and enthalpy (*b*) in the channel exit section for three gases: air (1), nitrogen (2), CO_2 (3)

Some conclusions from the computation results for three working gases in VGU-4 plasmatron for the two power regimes $N_{ap} = 45$ and 70 kW.

The difference in plasma parameters for the three gases are essential in general. Flow velocity u_{c0} and enthalpy h_{c0} in the channel exit section at the symmetry axis have maximum values for nitrogen and minimal values for CO_2 for both power regimes. Radial profiles $u_c(r)$ at the channel exit section for nitrogen and air are close to each other for both power regimes, and profiles $u_c(r)$ for CO_2 lay much lower. Also, maximum temperature values within the inductor region are greater for nitrogen and air and lower for CO_2 gas.

4.   Conclusion

Both experimental study and CFD modeling are fulfilled for investigation of quartz tube thermal state and subsonic ICP flow parameters in VGU-4 discharge channel for the two power regimes of $N_{ap} = 45$ and 70 kW for three working gases.

Temperature fields of quartz discharge channel were measured for all working gases. For the case of air this temperature fields were averaged and approximated to be used in boundary conditions in CFD modeling.

CFD modeling was made on the basis of Navier − Stokes and simplified Maxwell equations just for the VGU-4 experimental conditions.

The comparison of the calculated flow parameters was made for air working gas for power $N_{ap} = 70$ kW, for the three variants of boundary conditions for the wall temperature: $T_w = 300$ K (standard); $T_w = 747$ K (averaged temperature measurements); and linear distribution of temperature along the quartz tube obtained from the approximation of the experimental measurements). The computations show that the influence of different quartz wall temperature boundary conditions on the gas flow parameters at the channel exit section is negligible.

CFD modeling was made for the two power regimes for the three working gases. From the comparison of isotherms for the three working gases, it can be noted that the temperatures in carbon dioxide plasma are lower at the same power both in the discharge region and at the exit section of the discharge channel. The calculation results of temperature fields for nitrogen and air plasma are close, which is in accordance with the experiment, where similar temperature fields were obtained.

Note that the calculated stream function isolines and isotherms (figs. 7–12) are in accordance with the schematic view proposed in 1969 by Yu.P. Raizer in [5].

Acknowledgments

References

1.   Babat, G. I., "Bezelektrodnyj razryad i nekotorye smezhnye problemy (Electrodeless discharge and some allied problems)," *Vestnik elektropromyshlennosti*, No. 3, 1942, pp. 47−51 [in Russian].

2.   Babat, G. I., "Electrodeless discharges and some allied problems," *Journal of the Institution of Electrical Engineers*. Part III: Radio and Communication Engineering, Institution of Engineering and Technology (IET), Vol. 94, No. 27, 1947, pp. 27−37.

3.   Reed, T. B., "Induction-coupled plasma torch," *Journal of Applied Physics*, Vol. 32. No. 5, 1961, pp. 821−824. https://doi.org/10.1063/1.1736112

4.   Reed, T. B., "Heat-Transfer Intensity from Induction Plasma Flames and Oxy-Hydrogen Flames," *Journal of Applied Physics*, Vol. 34, No. 8, 1963, pp. 2266−2269. https://doi.org/10.1063/1.1702726

5.   Raizer, Yu. P., "High-Frequency High-Pressure Induction Discharge and the Electrodeless Plasmatron," *Soviet Physics Uspekhi*, Vol. 12, No. 6, 1970, pp. 777–791.

6. Kononov, S. V., Yakushin, M. I., "Heat transfer in a high-frequency electrodeless plasmatron operating in air," *Journal of Applied Mechanics and Technical Physics*, Vol. 7, No. 6, 1966, pp. 45−46. https://doi.org/10.1007/BF00914332

7. Yakushin, M. I., "Obtaining high gas temperatures in an electrodeless high-frequency discharge," *Journal of Applied Mechanics and Technical Physics*, Vol. 10, No. 3, 1969, pp. 470−478. https://doi.org/10.1007/BF00916183

8. Gordeev, A. N., Kolesnikov, A. F., Yakushin, M. I., "Induction plasma application to Buran's heat protection tiles ground tests," *SAMPE Journal*, Vol 28, No. 3, 1992.

9. Gülhan, A., Vennemann, D., Yakushin, M., Zhestkov, B., "Comparative oxidation tests on reference material in two induction heated facilities," *Acta astronautica*, Vol. 38, No. 4−8, 1996, pp. 501−509. https://doi.org/10.1016/0094-5765(96)00029-X

10. Kolesnikov, A. F., Gordeev, A. N., Vasilevskii, S. A., "Capabilities of RF-Plasmatron IPG-4 for re-entry simulation," *Journal of technical physics*, Vol. 50, No. 3, 2009, pp. 181−198.

11. Gordeev, A. N., "Over view of characteristics and experiments in IPM plasmatrons," VKI, RTOAVT, 1999.

12. Gordeev, A. N., Pershin, I. S., Yakushin, M. I., "Heat Regimes of Quartz Discharge Channel of Powerful Induction Plasmatron IPG-3-200," *Environmental Testing for Space Programs*, Vol. 408, 1997, p. 189.

13. Touloukian, Y. S., DeWitt, D. P., "Thermophysical properties of matter," *The TPRC data series,* Vol. 8. Thermal radiative properties-nonmetallic solids. 1972.

14. Baronets, P. N., Bykova, N. G., Gordeev, A. N., Pershin, I. S., Yakushin, M. I., "Experimental characterization of induction plasmatron for simulation of entry into Martian atmosphere," *Aerothermodynamics for space vehicles*, Vol. 426, 1999, p. 421.

15. Surzhikov, S. T., *Teplovoe izluchenie gazov i plazmy* (Thermal radiation of gases and plasma), Publishing House of the BMSTU, 2004, 543 p. [in Russian]

16. Vanden Abeele, D., Vasil'evskii, S. A., Kolesnikov, A. F., Degrez, G., Bottin, B., "Code-to-code validation of inductive plasma computations," *Progress in Plasma Processing of Materials*. Eds. P. Fauchais and J. Amouroux, Begell House, N.Y., 1999, pp. 245−250.

17. Rini, P., Vasil'evskii, S. A., Kolesnikov, A. F., Chazot, O., Degrez, G., "Inductively coupled CO_2 plasma flows: code-to-code comparison," *4-th International Symposium Atmospheric Reentry Vehicles and Systems*, 21-23 March 2005, Arcachon, France. Published also in VKI RP 2005-57.

18. Utyuzhnikov, S. V., Konyukhov, A. F., Vasil'evskii, S. A., Rudenko, D. V., Kolesnikov, A. F., Chazot, O., "Simulation of sub- and supersonic flows in inductive plasmatrons," *AIAA Journal*, Vol. 42, No. 9, 2004, pp.1871−1877. https://doi.org/10.2514/1.1195

19. Sakharov, V. I., Kolesnikov, A. F., Gordeev, A. N., Verant, J.-L., "CFD modeling of thermally and chemically nonequilibrium flows in discharge channel in subsonic plasmatron jets of the flat-face model," *Proceedings of the 6th European Symposium on Aerothermodynamics for Space Vehicles*, November 2008, Versailles, France. ESA SP-659.

20. Bykova, N. G., Vasil'evskii, S. A., Kolesnikov, A. F., "The effect of radiation on the spatial distribution of the temperature of subsonic flows of induction plasma," *High Temperature*, Vol. 42, No. 1, 2004, pp. 12−19. https://doi.org/10.1023/B:HITE.0000020086.83847.cd

21. Boulos, M. I., "Flow and temperature fields in the fire-ball of an inductively coupled plasma," *IEEE Trans. on Plasma Sc*. PS-4, 1976, Vol. 1, p. 28.

22. Vasil'evskii, S. A., Kolesnikov, A. F., Kubarev, S. N., Makarov, B. P., Yakushin, M. I., "Nonequilibrium flow and heat transfer in induction plasma generators," *Heat Transfer Research*, Vol. 25, No. 3, 1993, p. 365.

23. Vasil'evskii, S. A., Kolesnikov, A. F., Yakushin, M. I., "Mathematical models for plasma and gas flows in induction plasmatrons," *Molecular Physics and Hypersonic Flows*, Edited by M. Capitelli. NATO ASI Series, Kluwer, Dordrecht, 1996, p. 495.

24. Kolesnikov, A. F., Vasil'evskii, S. A., "Some problems of numerical simulation of discharge electrodynamics in induction plasmatron," *Proceedings of 15th IMACS World Congress*, Berlin, August 1997. Vol.3, *Computational Physics, Chemistry and Biology*. Ed. by A. Sydov, 1997, p. 175.

25. Vanden Abeele, D., Degrez, G., "Iterative methods for inductive plasma computations," *AIAA/ASME 7th Joint Thermophysics and Heat Transfer Conference*, AIAA Paper 98-2825, June 1998.

26. Vasilevskii, S. A., Kolesnikov, A. F., Bryzgalov, A. I., Yakush, S. E., "Computation of inductively coupled air plasma flow in the torches," *Journal of Physics: Conference Series*, Vol. 1009, 2018. p. 012027.

27. Sokolova, I. A., Vasil'evskii, S. A., Andriatis, A. V., "Computation of transport coefficients for multicomponent gas and plasma," *Physical-Chemical Kinetics in Gas Dynamics*, Vol. 3, 2005. http://chemphys.edu.ru/issues/2005-3/articles/80/ [in Russian]

28. Gurvich, L. V., at al., *Thermodynamic properties of individual substances*. I−IV volumes. Ed. Glushko V.P. Moscow, Nauka Publ. 1979−1982 [in Russian].

29. Kolesnikov, A.F, Tirskiy, G. A., "Equations of hydrodynamics for partially ionized multicomponent mixtures of gases, employing higher approximations of transport transfer coefficients," *Fluid Mechanics* - Soviet Research, Scripta Technica Publ., Vol. 13, No. 4, 1984, pp. 70–97.

30. Vasil'evskii, S. A., Sokolova, I. A., and Tirskii, G. A., "Exact equations and transport coefficients for a multicomponent gas mixture with a partially ionized plasma," *Journal of Applied Mechanics and Technical Physics*. Vol. 25, No. 4, 1984, pp. 510−519.

31. Vasil'evskii, S. A., Sokolova, I. A., and Tirskii, G. A., "Definition and computation of effective transport coefficients for chemical-equilibrium flows of partially dissociated and ionized gas mixtures," *Journal of Applied Mechanics and Technical Physics*, Vol. 27, No. 1, 1986, pp. 61−71.

32. Devoto, R. S., "Transport properties of ionized monoatomic gases," *Physics of Fluids*, Vol. 9, No. 6, 1966, pp.1230−1240.

33. Sokolova, I. A., "Computer library of transport properties for atmosphere gases and plasma," *Mathematical Modeling*, Vol. 10, No. 2, 1998, pp. 25−40 (translated from Russian)

34. Sokolova, I. A., "Modeling the molecular transfer for multicomponent gases and plasmas," Thesis. Moscow, 1992, 230 p. [in Russian].

35. Patankar, S. V., Spalding, D. B., "A calculation procedure for heat, mass and momentum transfer in three-dimensional parabolic flows," *International Journal of Heat and Mass Transfer*, Vol. 15, 1972, p. 1787.

36. Patankar, S., *Numerical heat transfer and fluid flow*, Hemisphere Publishing Corp. N.Y. 1980.

37. Vasil'evskii, S. A., Kolesnikov, A. F., "Numerical Simulation of Equilibrium Induction Plasma Flows in a Cylindrical Plasmatron Channel," *Fluid Dynamics*, Vol. 35, No. 5, 2000, pp. 769−777. https://doi.org/10.1023/A:1026659419493